Supporting Information

Cyclopropenylidenes as Strong Carbene Anchoring Groups on Au Surface

Evan A. Doud[1†], Rachel L. Starr[1†], Gregor Kladnik[4,5†], Anastasia Voevodin[1†], Enrique Montes[3], Narendra P. Arasu[3], Yaping Zang[2], Percy Zahl[8], Alberto Morgante[4,7*], Latha Venkataraman[1,2*], Héctor Vázquez[3*], Dean Cvetko[4,5,6*], Xavier Roy[1*]

[1] *Department of Chemistry and* [2] *Department of Applied Physics, Columbia University, New York, New York, 10027, United States*
[3] *Institute of Physics, Czech Academy of Sciences, Cukrovarnická 10, Prague 16200, Czech Republic*
[4] *CNR-IOM Laboratorio Nazionale TASC, Basovizza SS-14, km 163.5, Italy*
[5] *Faculty of Mathematics and Physics, University of Ljubljana, Jadranska 19, Ljubljana, Slovenia*
[6] *J. Stefan Institute, Jamova 39, SI-1000, Ljubljana, Slovenia*
[7] *Department of Physics, University of Trieste, via A. Valerio 2, 34127, Trieste, Italy*
[8] *Center for Functional Nanomaterials, Brookhaven National Laboratory, Upton, NY, 11973, USA*

[†] These authors contributed equally

[*] Correspondence:
morgante@iom.cnr.it (A. M.)
lv2117@columbia.edu (L. V.)
vazquez@fzu.cz (H. V.)
cvetko@iom.cnr.it (D. C)
xr2114@columbia.edu (X. R.)

Table of Contents:

1. Synthesis of BAC–CO_2 Precursor

BAC–CO_2 was synthesized following a previously reported literature procedure[1] starting from bis(diisopropylamino)cyclopropenium tetrafluoroborate [BAC][BF_4], also prepared via a literature procedure.[2] Briefly, [BAC][BF_4] was deprotonated with potassium bis(trimethylsilyl)amide (KHMDS) in diethyl ether to form the free BAC. After removal of the solvent in vacuo, the free carbene was dissolved in hexanes and filtered. Carbon dioxide was bubbled through the hexanes solution to generate the adduct, BAC–CO_2, which precipitates from solution as a white solid. Unlike the free carbene, BAC–CO_2 is air stable, affording new opportunities as a precursor in various synthetic strategies.

2. Computational Details

Calculation of carbene molecules adsorbed on the Au(111) surface.

The adsorption properties and electronic structure of BAC and NHC molecules on the Au(111) surface were calculated using the SIESTA implementation of density functional theory (DFT).[3] The non-local vdW-DF functional of Dion *et al.* which includes van der Waals (vdW) interactions in the implementation of Román-Pérez and Soler[4-5] was employed. The unit cell for calculations consists of three Au(111) layers, each containing 36 atoms, plus the molecule, and a vacuum gap of at least 10 Å (Figure S1). Molecular (gold) atoms were described using a double-ζ (single-ζ) polarized basis set. Reciprocal space was sampled using a 2×2×1 Monkhorst pack grid and a real-space grid was defined with an equivalent cut-off energy of 250 Ry. The coordinates of molecular and Au surface atoms were relaxed until the Hellmann-Feynman forces acting on these atoms were smaller than 0.02 eV/Å. The tilt angle (θ) is fixed by constraining the relative position of the atoms in the cyclopropenylidene ring. The position of these atoms was kept fixed relative to each other, without restricting their displacement as a rigid unit. The tilt angle is defined as the angle between the plane of the cyclopropenylidene ring and the z axis. For the calculation of the binding energy, corrections to basis set superposition errors were taken into account. The binding energy for the fully unconstrained geometry is -1.72 eV, slightly higher than the geometries with constrained angle. The contribution of dispersion interactions to the binding energy was computed for the most stable BAC geometry (θ = 40°) from the difference to a PBE calculation at the same geometry. We found a contribution of -1.40 eV to the total binding energy of -1.65 eV of BAC at θ = 40°. The binding energy of DAC at the same angle (θ = 40°) was calculated to be -1.16 eV, of which -0.93 eV corresponds to van der Waals interactions.

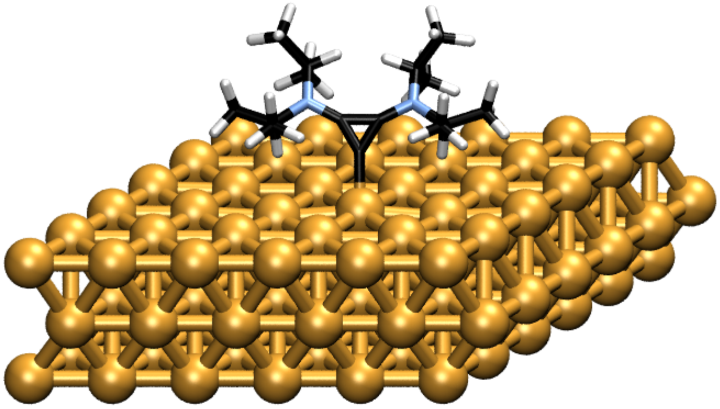

Figure S1: Unit cell used in the DFT calculations of the adsorbed molecule.

Calculation of isolated molecule and carbene-Au atom complexes.

The electronic properties of diaminocyclopropenylidene (DAC) and dihydroimidazol-2-ylidene (NHC) molecules as well as DAC-Au_1 and NHC-Au_1 complexes in the gas phase were calculated with Gaussian.[6] Exchange-correlation was approximated with the B3LYP functional. 6-31G* (LANL2DZ) basis sets were used to describe the Au atoms. The total energy of DAC-Au_1 and NHC-Au_1 complexes was calculated as a function of the angle between the C-Au bond and the carbene planes, as shown in Figure S2a for the DAC-Au_1 complex. This angle was constrained while all other degrees of freedom were optimized. Figure S2b shows the calculated energy profiles, with the energy at 0 degrees in each case set to zero for ease of comparison. While the most stable geometry of NHC-Au is found for 0 degrees, the lowest energy of the DAC-Au complex is obtained when the C-Au bond is tilted 24 degrees from the carbene plane. Thus, the possibility of DAC to bind at a tilted angle develops already with a single Au atom.

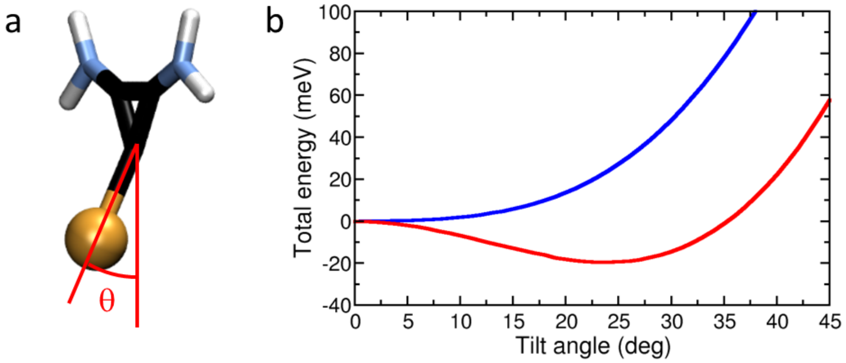

Figure S2: a) Structure of the DAC -Au complex used in the calculations. b) Energy of DAC -Au (red curve) and NHC-Au (blue curve) complexes as a function of tilt angle, relative to the value at 0 degrees.

To elucidate the origin of the out of plane binding in DAC but not in NHC, the electrostatic potential of isolated DAC and NHC molecules was calculated. Figure S3a shows the calculated electrostatic potential of DAC (top) and NHC (bottom) isolated molecules. Contour lines are plotted at 1, 10, and 20 eV. The position of the Au atom at its most stable conformation in Figure S3 is indicated by a cross. In Figure S3b, the three-dimensional electrostatic potential is represented in real-space projected onto an isosurface of the electron density (10^{-3} e/Å^3). Positive (negative) values of the potential, corresponding to blue (red) regions, indicate electron-deficient (electron-rich) regions of the molecule. The broader angular distribution in DAC compared to NHC evidences its ability to bond to Au in a tilted conformation.

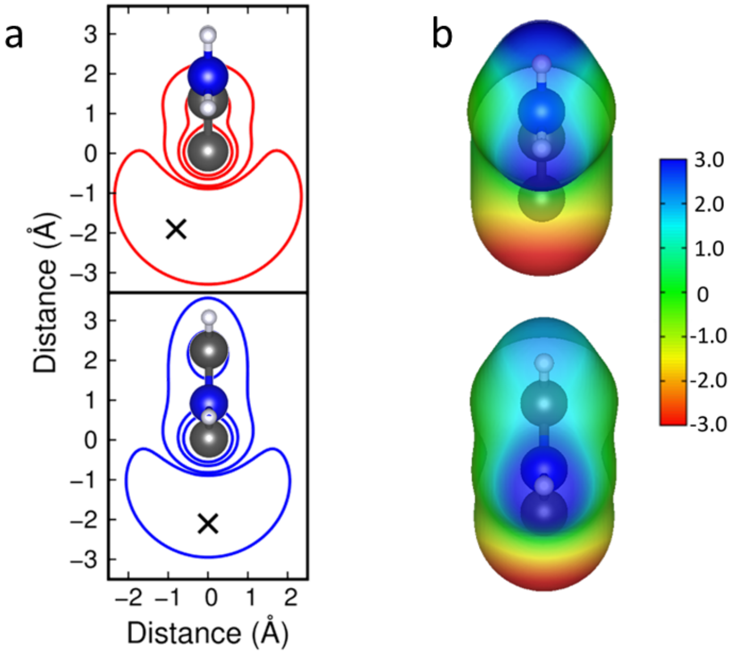

Figure S3: a) Electrostatic potential contour lines of DAC and NHC. b) Real-space representation for DAC (top) and NHC (bottom) of the electrostatic potential (in V) projected over the electron density isocontour (10^{-3} e/Å^3) .

3. Details of XPS and NEXAFS Measurements

The X-ray photoemission (XPS) and absorption (NEXAFS) measurements were performed at the ALOISA beamline[7] of the Elettra synchrotron. The Au(111) surface was prepared by cycles of Ar^+ sputtering (1.5 keV) and thermal annealing up to ~750 K. Absence of surface contaminants was checked by XPS prior to molecule deposition. The BAC precursor was loaded into a pyrex cell and pumped down to high vacuum resulting in decarboxylation and sublimation of the carbene compounds for deposition. During the deposition the cell was heated to ~380 K and the sample chamber pressure reached 2×10^{-8} mbar. The temperature of the Au substrate was controlled during the deposition (as reported in the text) and then cooled down to ~200 K for the X-ray absorption measurement.

XPS spectra were taken at grazing incidence angle (4°) using a photon energy of 500 eV with the photon electric field aligned 4° off the surface normal. The emitted electrons were detected by a hemispherical electron analyzer in normal emission geometry, with overall energy resolution better than 220 meV. The binding energy scale has been calibrated using bulk spectral component of the Au $4f_{7/2}$ peak at 84.0 eV.[8]

Figure S4 shows the XPS measurement of the BAC film deposited on Au(111) surface held at 370 K sample temperature. We detect no oxygen spectral features indicating that the CO_2 moiety in the precursor molecules is cleaved off leaving just the BAC molecule deposited on the substrate.

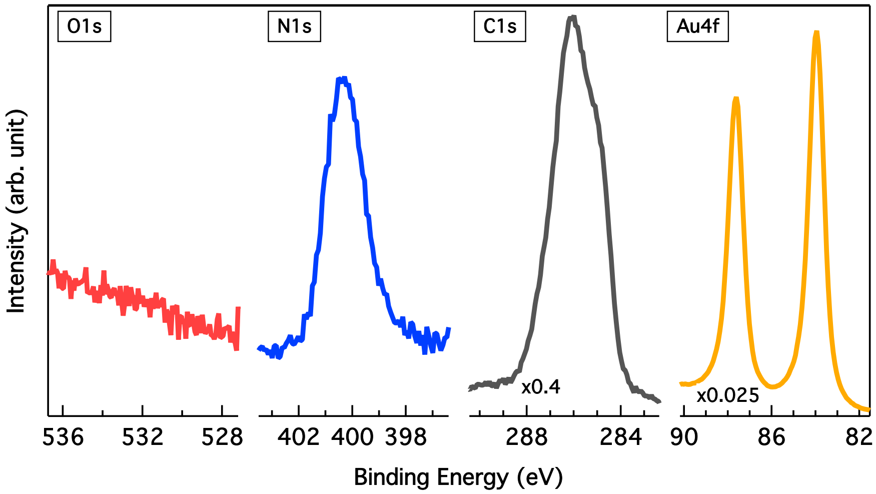

Figure S4: XPS measurement of the as-deposited BAC film at 370 K sample temperature. Lack of any oxygen signal indicates that CO_2 moiety is cleaved from the precursor molecules. Intensities of the C1s and Au4f spectral features are scaled as indicated for better comparison.

The effect of temperature annealing the BAC film is further shown in Figure S5 and S6. Some N1s and C1s signals are reduced after annealing to 430 K and 470 K, pointing to a partial desorption of the BAC. The C1s peak shape in the as deposited film displays two distinct components at 285.2 and 286.0 eV, with the higher binding energy component likely due to bilayer formation where substrate screening of the core hole is less efficient. The C1s peak profile of the 430 K and 470 K annealed film demonstrates that predominantly the high binding energy component is reduced, whereas the low binding energy component is preserved. The slight increase of the Au4f signal upon temperature annealing also indicates that some of the BAC molecules desorb, leaving just the monolayer.

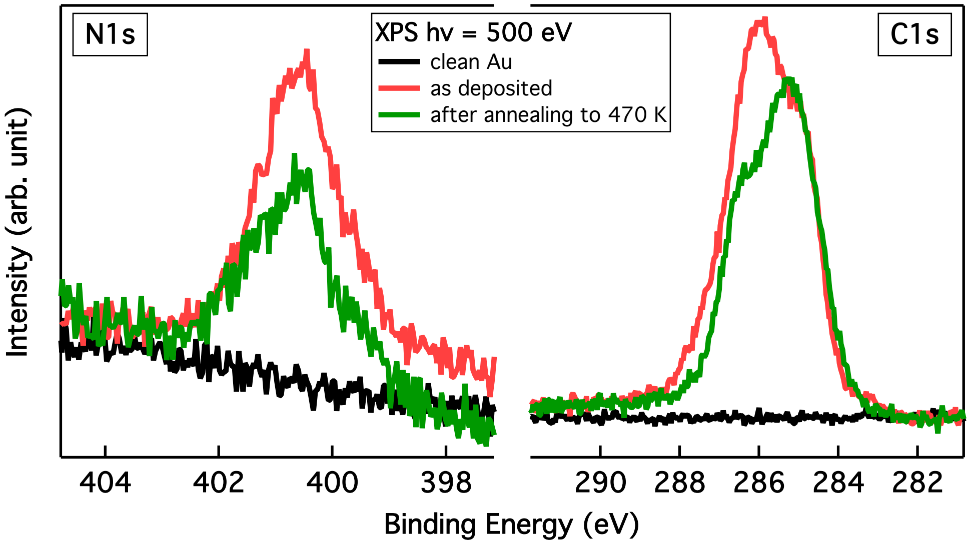

Figure S5: N1s and C1s XPS data of BAC film deposited on Au(111) (red) and after temperature annealing to 470 K (green). Changes in the C 1s peak shape indicate desorption of the second layer leaving just a single layer of BAC on Au. Clean gold substrate XPS scans are also shown (black) as a reference.

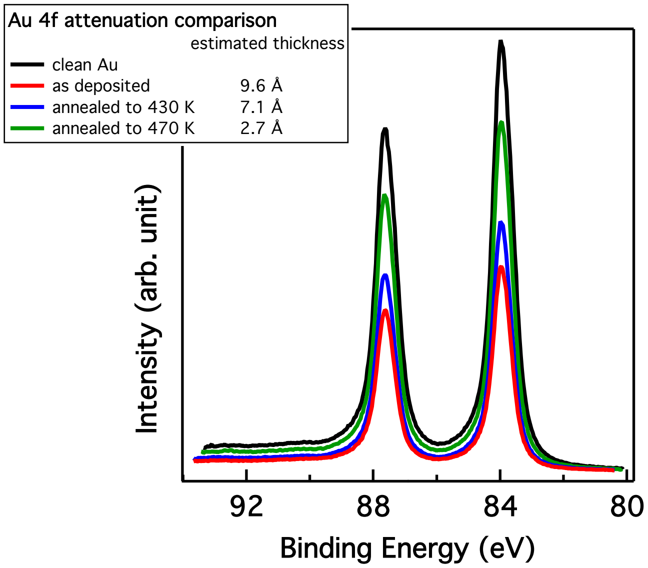

Figure S6: Comparison of Au 4f intensity attenuation due to different thicknesses of the BAC film remaining after temperature annealing the pristine (as deposited) film.

The NEXAFS N K-edge spectra were acquired in partial electron yield mode by a wide acceptance angle channeltron detector. A grid placed in front of the channeltron was polarized to -370 V, acting as a high-pass filter rejecting electrons with kinetic energies lower than 370 eV. The photon energy resolution was better than 150 meV. Polarization dependent NEXAFS spectra were taken in two polarizations, in *p*-polarization (photon electric field normal to the surface) and *s*-polarization (electric field parallel to the surface), to measure the molecular adsorption geometry.[9] Magic angle NEXAFS spectra were measured with the surface normal at 55 degrees from the photon polarization.

4. Details of DFT Calculations of X-ray Photoemission and Absorption Spectra

We simulate the effect of gold adatoms or step edges by introducing a gold dimer as shown in Figure S7 and optimizing the geometry using density functional theory (DFT) with the B3LYP functional and the double-zeta correlation-consistent basis set (cc-pVDZ) implemented in the NWChem computational chemistry package.[10] The optimized geometry then served as input to GPAW, a DFT Python code based on the projector-augmented wave (PAW) method to calculate the core electron binding energies (CEBEs) as well as the X-ray absorption spectra (XAS).[11-13]

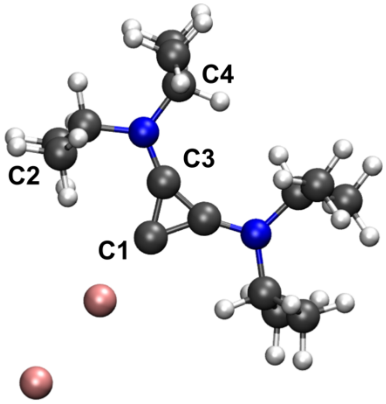

Figure S7: Optimized geometry of the BAC molecule with a gold dimer near the C1 carbene carbon.

We calculated the CEBEs of all inequivalent C1s sites with the PBE functional with a cell size of 25.6 Å and grid spacing of 0.2 Å using the delta Kohn-Sham scheme. The full core-hole PAW setups were created with GPAW and default parameter values. The inequivalent C1s sites are marked in Figure S7 and correspond to the carbene carbon (C1), aromatic carbons bound to nitrogen (C3), aliphatic carbons also bound to nitrogen (C4) and aliphatic carbons (C2) in the propyl groups. Figure S8a shows a comparison of the calculated C1s (blue) CEBEs with the measured XPS (green) after flashing the deposited film to 420K. The shape of the C1s peak changed significantly upon flashing to 430 K (compare with Figure S4) probably indicating desorption of the second layer. This is further corroborated by the DFT calculation of the C1s CEBEs. The calculated CEBEs were offset to match the measured XPS for better comparison and the intensities were set to follow the expected stoichiometric ratios. The simulated peak shapes were obtained by gaussian convolution with FWHM = 0.4 eV.

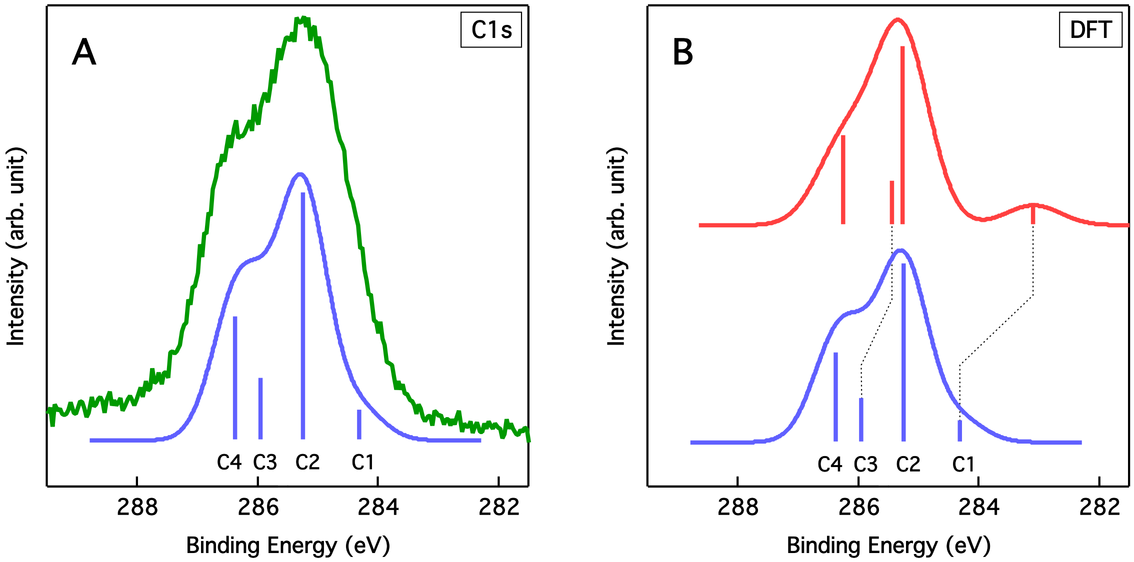

Figure S8: **a)** Comparison of the measured C1s peak (green) with the calculated CEBEs, which are shifted to match the measured peak position. **b)** Comparison of the calculated CEBEs for isolated BAC molecule (red) and the BAC molecule with a gold dimer placed near the carbene (C1) carbon.

The overall peak shape is well reproduced in the DFT calculation of the BAC molecule with an Au dimer. The effect of the Au dimer on the spectra are shown in the Figure S8b with the isolated BAC molecule CEBEs shown in red and the BAC with Au dimer CEBEs shown in blue. The calculated energies were offset to match the main (C2) component position belonging to the propyl group atoms presumably least prone to modification due to coupling with the Au dimer. The CEBEs of the peaks corresponding to the carbons closest to the Au dimer (C1 and C3) are found shifted towards higher binding energies relative to the positions of the other two peaks indicating a charge redistribution from the molecule's carbene core to the Au dimer.

X-ray absorption spectra (NEXAFS) were performed using the half core-hole transition potential method as implemented in GPAW. The calculation parameters were the same as for the CEBE calculations described above. The calculated NEXAFS spectra were obtained by gaussian convolution of the calculated transition intensities represented in the corresponding figures by sticks. We focus only on nitrogen K-edge NEXAFS spectra, since the measured carbon K-edge spectrum, Figure S9b, has a rich fine structure, due to the different initial states (C1-C4) where the majority of the signal stems from the aliphatic carbons. The contribution of the aromatic (and carbene) carbons is minimal and their effect on the measured absorption spectra is experimentally difficult to evaluate.

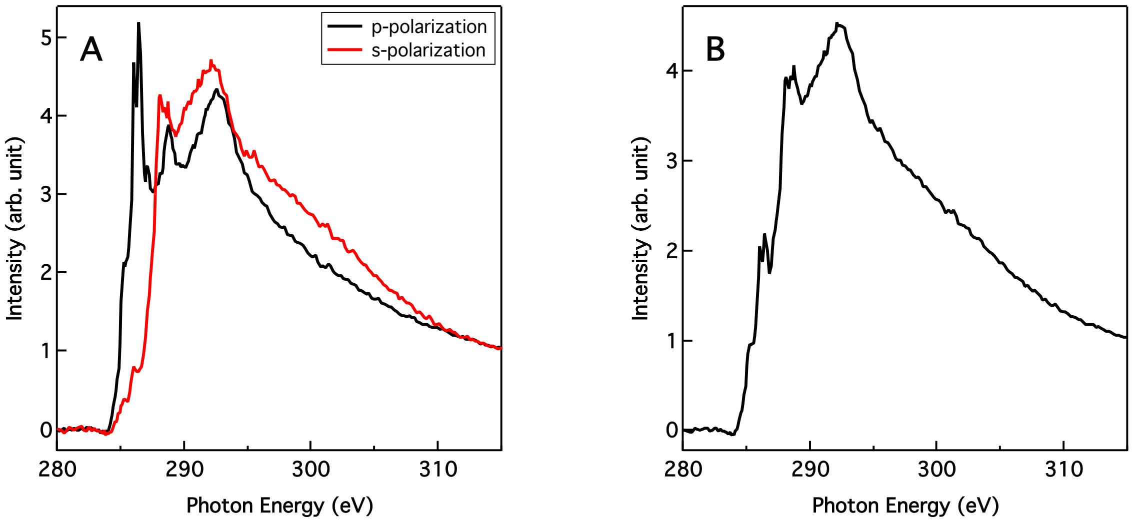

Figure S9: **a)** Polarization dependent carbon K-edge NEXAFS of the flashed BAC film and **b)** the corresponding magic angle NEXAFS.

Nitrogen K-edge spectra are easier to simulate since both N atoms in the molecule are equivalent. Moreover, the N atoms are directly bound to the aromatic (carbene) core indicating that electronic structure changes localized on the aromatic core should manifest also in nitrogen related unoccupied orbitals. Additionally, as noted in the main text, the DFT calculations of the BAC geometry show that the aromatic carbons (C1 and C3) and the nitrogens lie almost in the same plane, which allows us to use the measured dichroism in the polarization dependent N K-edge NEXAFS to estimate the orientation of the aromatic (carbene) core of the molecule relative to the substrate plane.

We calculate NEXAFS in magic angle conditions, i.e. absorption spectra independent of the molecular orientation, since we are specifically interested in the unoccupied molecular states and the corresponding transition energies. Experimentally we observe a significant change in the absorption spectra, where it appears that the LUMO peak position shifts toward lower excitation energy upon flash annealing the deposited film to 430 K (see main text Figure 2b). We attribute this to reorganization of the BAC molecules on the Au substrate surface toward more reactive sites (Au adatoms, step edges). This is further corroborated by our DFT simulations where we investigate the effect of the distance between the gold dimer and the C1 (carbene) carbon on the simulated N K-edge NEXAFS, Figure S10.

In Figure S10a we compare the experimentally derived magic angle N K-edge NEXAFS data (top black and red traces) with the DFT calculated NEXAFS spectra for isolated BAC molecule and BAC molecule with a gold dimer positioned at different distances to the C1 (carbene) carbon. Of immediate note, the peak at ~398 eV in the measured spectra is attributed to synchrotron beam induced modification of the amino groups and is therefore not reproduced in the DFT calculations. The calculated NEXAFS spectra were obtained by gaussian convolution of the calculated transition intensities represented in the figure by sticks. The calculated absorption spectrum of isolated BAC molecule (yellow trace) reproduces the NEXAFS measured just after deposition very well. The as deposited film is a multilayer, as established from the XPS data, therefore no features induced by molecule-substrate interactions are expected in the spectrum and is confirmed by the DFT calculation. The addition of a gold dimer induces some charge delocalization from the molecule to the gold dimer as indicated by the bubble plots shown in the Figure S10b. This further induces a transition energy shift of the LUMO orbital to lower energies, which reaches a minimum for a gold – carbon distance of about 2.0Å (red trace). This shift is indeed observed in the measured spectra, where after flashing to 430 K the NEXAFS changes significantly, with a shift of the peak at ~402 eV (black trace) to an energy of ~400.5 eV. Our DFT calculations show that this shift can be attributed to stronger Au substrate – BAC molecule interaction. Although the full -1.5 eV shift is not reproduced with our calculations, the trend is clear – stronger interaction, i.e. smaller distance between the C1 carbene carbon and the gold dimer, yields a larger shift of the LUMO excitation energy towards lower values.

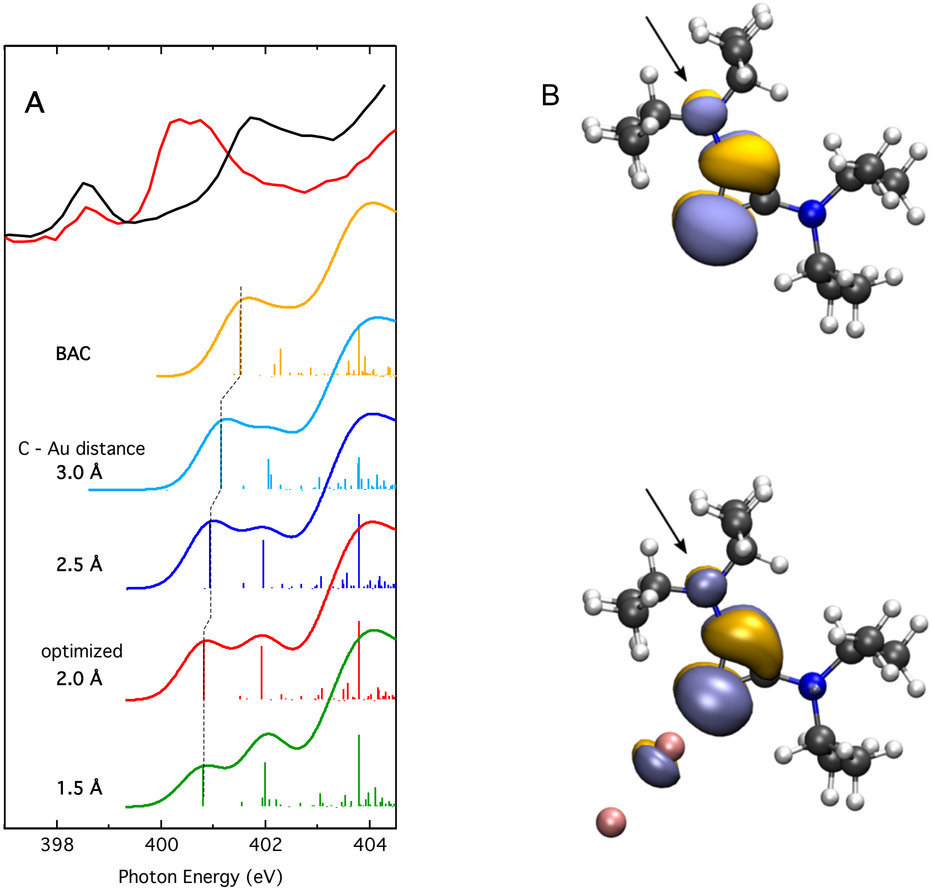

Figure S10: **a)** Comparison of experimentally derived magic-angle N K-edge NEXAFS (top black after BAC deposition, top red after flash to 430 K) and DFT calculated NEXAFS spectra of isolated BAC molecule (yellow) and BAC molecule with a gold dimer at different distances from the C1 (carbene) carbon. **b)** Bubble plot of the calculated "LUMO" with a half-core-hole on the nitrogen atom pointed on with an arrow for the isolated BAC molecule (top right) and the BAC molecule with a gold dimer (bottom right).

5. Scanning probe microscopy experiments:

Measurements were performed with a Createc-based low-temperature (LT)-STM system custom upgraded (by the author P. Zahl) with NC-AFM capability and operated using the open source GXSM control software.[14-16] Our Q-Plus sensor used for the STM/NC-AFM measurements has a 25 µm PtIr tip wire attached which was cut and sharpened by a focused ion beam (FIB) milling following a final cleaning procedure in UHV using Ar^+ sputtering from three directions before mounting on the SPM scanner.

Simulation of AFM images.

AFM images were calculated using the probe particle model[17] for the BAC structure at $\theta = 40°$. The parameters of the tip were chosen to simulate a CO-functionalized tip (lateral stiffness of 0.24 N/m). Images were generated by scanning the tip over BAC on a three-dimensional grid with a spacing of 0.1 Å. At each grid position of the vertical approach, the tip position was allowed to relax. An oscillation amplitude of around 1 Å was used.

6. References

(1) Kuchenbeiser, G.; Soleilhavoup, M.; Donnadieu, B.; Bertrand, G. Reactivity of Cyclic (Alkyl)(amino)carbenes (CAACs) and Bis(amino)cyclopropenylidenes (BACs) with Heteroallenes: Comparisons with their N-Heterocyclic Carbene (NHCs) Counterparts. *Chem. Asian J.* **2009,** *4*, 1745-1750. DOI: 10.1002/asia.200900338.

(2) Lavallo, V.; Ishida, Y.; Donnadieu, B.; Bertrand, G. Isolation of cyclopropenylidene-lithium adducts: The Weiss-Yoshida reagent. *Angew. Chem. Int. Ed.* **2006,** *45*, 6652-6655. DOI: 10.1002/anie.200602701.

(3) Soler, J. M.; Artacho, E.; Gale, J. D.; Garcia, A.; Junquera, J.; Ordejon, P.; Sanchez-Portal, D. The SIESTA method for ab initio order-N materials simulation. *J. Phys. Condens. Matter.* **2002,** *14*, 2745-2779. DOI: 10.1088/0953-8984/14/11/302.

(4) Dion, M.; Rydberg, H.; Schroder, E.; Langreth, D. C.; Lundqvist, B. I. Van der Waals density functional for general geometries. *Phys. Rev. Lett.* **2004,** *92*, 246401. DOI: 10.1103/PhysRevLett.92.246401.

(5) Roman-Perez, G.; Soler, J. M. Efficient Implementation of a van der Waals Density Functional: Application to Double-Wall Carbon Nanotubes. *Phys. Rev. Lett.* **2009,** *103*, 096102. DOI: 10.1103/PhysRevLett.103.096102.

(6) Frisch, M. J.; Trucks, G. W.; Schlegel, H. B.; Scuseria, G. E.; Robb, M. A.; Cheeseman, J. R.; Scalmani, G.; Barone, V.; Petersson, G. A.; Nakatsuji, H.; Li, X.; Caricato, M.; Marenich, A. V.; Bloino, J.; Janesko, B. G.; Gomperts, R.; Mennucci, B.; Hratchian, H. P.; Ortiz, J. V.; Izmaylov, A. F.; Sonnenberg, J. L.; Williams; Ding, F.; Lipparini, F.; Egidi, F.; Goings, J.; Peng, B.; Petrone, A.; Henderson, T.; Ranasinghe, D.; Zakrzewski, V. G.; Gao, J.; Rega, N.; Zheng, G.; Liang, W.; Hada, M.; Ehara, M.; Toyota, K.; Fukuda, R.; Hasegawa, J.; Ishida, M.; Nakajima, T.; Honda, Y.; Kitao, O.; Nakai, H.; Vreven, T.; Throssell, K.; Montgomery Jr., J. A.; Peralta, J. E.; Ogliaro, F.; Bearpark, M. J.; Heyd, J. J.; Brothers, E. N.; Kudin, K. N.; Staroverov, V. N.; Keith, T. A.; Kobayashi, R.; Normand, J.; Raghavachari, K.; Rendell, A. P.; Burant, J. C.;

Iyengar, S. S.; Tomasi, J.; Cossi, M.; Millam, J. M.; Klene, M.; Adamo, C.; Cammi, R.; Ochterski, J. W.; Martin, R. L.; Morokuma, K.; Farkas, O.; Foresman, J. B.; Fox, D. J. *Gaussian 16 Rev. A.03*, Wallingford, CT, 2016.

(7) Floreano, L.; Naletto, G.; Cvetko, D.; Gotter, R.; Malvezzi, M.; Marassi, L.; Morgante, A.; Santaniello, A.; Verdini, A.; Tommasini, F.; Tondello, G. Performance of the grating-crystal monochromator of the ALOISA beamline at the Elettra Synchrotron. *Rev. Sci. Instrum.* **1999,** *70*, 3855-3864. DOI: 10.1063/1.1150001.

(8) Cossaro, A.; Floreano, L.; Verdini, A.; Casalis, L.; Morgante, A. Comment on ``Local Methylthiolate Adsorption Geometry on Au(111) from Photoemission Core-Level Shifts''. *Phys. Rev. Lett.* **2009,** *103*, 119601. DOI: 10.1103/PhysRevLett.103.119601.
(9) Stöhr, J., *NEXAFS Spectroscopy*. Springer-Verlag Berlin Heidelberg: New York, 1992; Vol. 25.

(10) Valiev, M.; Bylaska, E. J.; Govind, N.; Kowalski, K.; Straatsma, T. P.; Van Dam, H. J. J.; Wang, D.; Nieplocha, J.; Apra, E.; Windus, T. L.; de Jong, W. NWChem: A comprehensive and scalable open-source solution for large scale molecular simulations. *Comput. PHys. Commun.* **2010,** *181*, 1477-1489. DOI: 10.1016/j.cpc.2010.04.018.

(11) Bahn, S. R.; Jacobsen, K. W. An object-oriented scripting interface to a legacy electronic structure code. *Comput. Sci. Eng.* **2002,** *4*, 56-66. DOI: 10.1109/5992.998641.

(12) Mortensen, J. J.; Hansen, L. B.; Jacobsen, K. W. Real-space grid implementation of the projector augmented wave method. *Phys. Rev. B.* **2005,** *71*, ARTN 035109. DOI: 10.1103/PhysRevB.71.035109.

(13) Enkovaara, J.; Rostgaard, C.; Mortensen, J. J.; Chen, J.; Dulak, M.; Ferrighi, L.; Gavnholt, J.; Glinsvad, C.; Haikola, V.; Hansen, H. A.; Kristoffersen, H. H.; Kuisma, M.; Larsen, A. H.; Lehtovaara, L.; Ljungberg, M.; Lopez-Acevedo, O.; Moses, P. G.; Ojanen, J.; Olsen, T.; Petzold, V.; Romero, N. A.; Stausholm-Moller, J.; Strange, M.; Tritsaris, G. A.; Vanin, M.; Walter, M.;

Hammer, B.; Hakkinen, H.; Madsen, G. K. H.; Nieminen, R. M.; Norskov, J.; Puska, M.; Rantala, T. T.; Schiotz, J.; Thygesen, K. S.; Jacobsen, K. W. Electronic structure calculations with GPAW: a real-space implementation of the projector augmented-wave method. *J. Phys. Condens. Matter.* **2010,** *22*. DOI 10.1088/0953-8984/22/25/253202.

(14) Zahl, P.; Wagner, T. GXSM - Smart & Customizable SPM Control. *Imaging & Microscopy* **2015,** 1, 38-41. DOI: 10.1002/imaging.4840.

(15) Zahl, P.; Klust, A. GXSM Software Project Homepage. http://gxsm.sourceforge.net/.

(16) Reineke, S.; Lindner, F.; Schwartz, G.; Seidler, N.; Walzer, K.; Lussem, B.; Leo, K. White organic light-emitting diodes with fluorescent tube efficiency. *Nature* **2009,** *459*, 234-U116. 10.1038/nature08003.

(17) Hapala, P.; Kichin, G.; Wagner, C.; Tautz, F. S.; Temirov, R.; Jelinek, P. Mechanism of high-resolution STM/AFM imaging with functionalized tips. *Phys. Rev. B.* **2014,** *90*. DOI: 10.1103/PhysRevB.90.085421